PERGAMON

International Journal of Solids and Structures 40 (2003) 4487–4500

INTERNATIONAL JOURNAL OF SOLIDS and STRUCTURES

www.elsevier.com/locate/ijsolstr

Shape optimization of impactor penetrating into concrete or limestone targets

G. Ben-Dor, A. Dubinsky, T. Elperin *

Pearlstone Center for Aeronautical Engineering Studies, Department of Mechanical Engineering, Ben-Gurion University of the Negev, P.O. Box 653, Beer-Sheva 84105, Israel

Received 30 July 2002

Abstract

The shape of the normally striking impactor that attains the maximum depth of penetration into a concrete or a limestone semi-infinite target for a given impact velocity is found. It is shown that the optimum shape is close to a blunt (in general case) cone and it is independent on the properties of the material of the target in the framework of the employed penetration model. The performance of some other typical shapes of the nose of the impactors (spherical-conic impactors, sharp-conic impactors, truncated-ogive impactors) are analyzed and compared with the optimal impactor.

Keywords: Optimization; Penetration; Optimum shape

1. Introduction

There are a few publications on impactor's shape optimization. In the first studies on this problems, indirect criteria of optimization were used, namely, the resistance in motion of the penetrator inside a target (Bunimovich and Yakunina, 1987a,b; Bunimovich, 1989; Ostapenko and Yakunina, 1992; Yankilevsky, 1983) and the "dynamical work" (Kusher, 1967); the latter approach is discussed by Nixdorff (1987) and Ben-Dor et al. (2001). More recently, the direct criteria, the maximum depth of penetration in the case of a semi-infinite target and the minimum ballistic limit velocity for a target with a finite thickness, was used. The results were obtained for ductile homogeneous targets (Ben-Dor et al., 2000, 2001, 2003; Vedernikov and Shchepanovsly, 1995; Ostapenko et al., 1994; Ostapenko and Yakunina, 1999; Yakunina, 2000, 2001; Jones et al., 1998; Jones and Rule, 2000; Bunimovich and Dubinsky, 1995) and layered shields (Ben-Dor et al., 1997, 1999) and fiber-reinforced plastic (FRP) laminates (Ben-Dor et al., 2002a,b). In this study we considered the problem of impactor's nose optimization applied to concrete and limestone targets.

* Corresponding author.
E-mail addresses: bendor@menix.bgu.ac.il (G. Ben-Dor), dubin@menix.bgu.ac.il (A. Dubinsky), elperin@menix.bgu.ac.il (T. Elperin).

0020-7683/03/$ - see front matter © 2003 Elsevier Ltd. All rights reserved.
doi:10.1016/S0020-7683(03)00212-9

2. Description of the model and formulation of the problem

Consider a normal penetration of a rigid striker (a body of revolution) into a concrete or limestone semi-infinite target. The notations are shown in Fig. 1. The coordinate h, the instantaneous depth of penetration, is defined as the distance between the nose of the impactor and the front surface of the target. The Cartesian coordinates xOy are associated with the impactor, the generator of the impactor is determined as $y = \Phi(x)$. As a basis in our study of optimization problem we used the two-step penetration model (Forrestal et al., 1994, 1996; Frew et al., 1998) that initially was suggested for concrete target.

At the first step of the penetration, the resistance force is

$$D = ch, \quad 0 \leqslant h \leqslant 4R, \tag{1}$$

where c is a constant.

At the second step ($h \geqslant 4R$), it is assumed that impactor–target interaction at a given location at the impactor's surface that is in contact with the target is determined by the following equation:

$$\mathrm{d}\vec{F} = \Omega(u)\vec{n}^0\,\mathrm{d}S, \quad u = -\vec{v}\cdot\vec{n}^0 = v\vec{x}^0\cdot\vec{n}^0, \tag{2}$$

where $\mathrm{d}\vec{F}$ is the forces acting at the nose and lateral surface elements $\mathrm{d}S$, $\vec{n}^0$ is the inner normal unit vector, $\vec{v}$ is a local velocity vector, $\vec{x}^0$ is an unit vector of x-axis (see Fig. 1), function Ω determines the model of impactor–target interaction. Assuming that the function Ω is the same for different impactor's shapes this function is determined from the solution of the problem of cavity expansion (Forrestal and Luk, 1992):

$$\Omega(u) = a_0 + b_0u^2. \tag{3}$$

In the case of a concrete target, $a_0 = sf'_c$, $b_0 = \gamma$, where f'_c and γ are the unconfined compressive strength and the density of the material of the target, respectively, dimensionless empirical constant s can be calculated using the following approximation (Frew et al., 1998) $s = 82.6(f'_c)^{-0.544}$ (f'_c in MPa). In the case of a limestone target (Frew et al., 2000), $b_0 = \gamma$, $a_0 = \mu_0 + \mu_1(R/R_0)$ where $\mu_0 = 607$ MPa, $\mu_1 = 86$ MPa, $R_0 = 0.0254$ m.

The model of Eqs. (2) and (3) is directly applicable to impactors with the flat thickness (Ben-Dor et al., 2001; Chen and Li, 2001, 2002), without recourse to artificial expedients taking into account the truncation effect (see, e.g., Qian et al., 2000). Let us derive the expression for the resistance force in the form that is convenient for a future analysis.

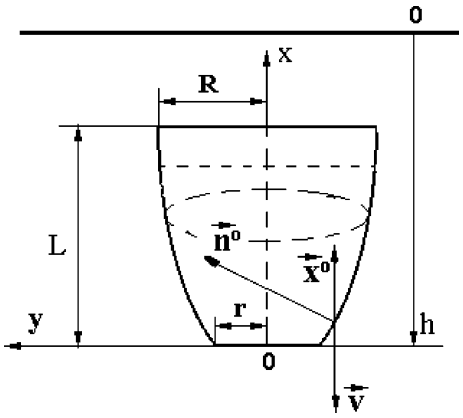

Fig. 1. Coordinates and notations.

The total force $\vec{F}$ is determined by integrating the local force over the flat thickness and the lateral surfaces, S_{flat} and S_{lat}, respectively. Using formulae from differential geometry and taking into account that $\vec{x}^0 \cdot \vec{n}^0 = 1$ at the flat thickness, the following expression for the resistance force can be derived:

$$D = \vec{x}^0 \left(\int_{S_{\text{nose}}} \mathrm{d}\vec{F}_{\text{nose}} + \int_{S_{\text{lat}}} \mathrm{d}\vec{F}_{\text{lat}} \right) = \pi(b_0 v^2 + a_0) r^2 + 2\pi \int_0^L \left(b_0 \frac{\Phi_x^2}{\Phi_x^2 + 1} v^2 + a_0 \right) \Phi_x \Phi \, \mathrm{d}x$$
$$= a + bv^2, \tag{4}$$

where

$$a = \pi a_0 (r^2 + \eta) = \pi a_0 R^2, \tag{5}$$

$$b = \pi b_0 \left[r^2 + 2 \int_0^L \left(\Phi \Phi_x - \frac{\Phi \Phi_x}{\Phi_x^2 + 1} \right) \mathrm{d}x \right] = \pi b_0 (r^2 + \eta - 2J) = \pi b_0 (R^2 - 2J), \tag{6}$$

$$\eta = 2 \int_0^L \Phi \Phi_x \, \mathrm{d}x = \int_0^L \frac{\mathrm{d}\Phi^2}{\mathrm{d}x} \mathrm{d}x = R^2 - r^2, \qquad \Phi_x = \frac{\mathrm{d}\Phi}{\mathrm{d}x}, \tag{7}$$

$$J = \int_0^L \frac{\Phi \Phi_x}{\Phi_x^2 + 1} \mathrm{d}x \tag{8}$$

and $r = \Phi(0)$, $R = \Phi(L)$ (see Fig. 1).

Let us derive the expression for the depth of penetration using a method that is less involved as compared to Forrestal and Luk (1992). Taking into account that

$$\frac{\mathrm{d}^2 h}{\mathrm{d}t^2} = \frac{\mathrm{d}v}{\mathrm{d}t} = \frac{1}{2} \frac{\mathrm{d}w}{\mathrm{d}h}, \qquad w(h) = v^2, \tag{9}$$

equation of motion of impactor with the mass m reads:

$$\frac{m}{2} \frac{\mathrm{d}w}{\mathrm{d}h} = -D, \quad D = \begin{cases} ch & \text{if } 0 \leqslant h \leqslant 4R, \\ a + bw & \text{if } h \geqslant 4R, \end{cases} \tag{10}$$

where the constant c is determined using condition of continuity of the resistance force at $h = 4R$:

$$4Rc = a + b\hat{w}, \qquad \hat{w} = w(4R). \tag{11}$$

Considering the motion of the impactor between the initial ($h = 0$, $w = v_0^2$, where v_0 is the impact velocity of the impactor) and the final ($h = 4R$, $w = \hat{w}$) locations of the first step of penetration Eq. (10) allows us to write:

$$\frac{m}{2} \int_{v_0^2}^{\hat{w}} \mathrm{d}w = -c \int_0^{4R} h \, \mathrm{d}h. \tag{12}$$

Calculating the integrals we obtain:

$$m(v_0^2 - \hat{w}) = (4R)^2 c. \tag{13}$$

In a similar manner, the equation of motion of the impactor between the point $h = 4R$, $w = \hat{w}$ and the point $h = H$, $w = 0$ (H is the depth of penetration (DOP), i.e., the depth when the impactor stops, and it is assumed that $H \gg 4R$) of the second step of penetration implies:

$$\frac{m}{2}\int_{\hat{w}}^{0}\frac{\mathrm{d}w}{a+bw}=-\int_{4R}^{H}\mathrm{d}h, \tag{14}$$

or

$$H=4R+\frac{m}{2}\int_{0}^{\hat{w}}\frac{\mathrm{d}w}{a+bw}=4R+\frac{m}{2b}\mathrm{Ln}\left(1+\frac{b}{a}\hat{w}\right). \tag{15}$$

Eliminating c from Eqs. (11) and (13) we arrive at the following formula for $\hat{w}$:

$$\hat{w}=\frac{mv_0^2-4aR}{m+4bR},\quad v_0^2>2\sqrt{\frac{aR}{m}}. \tag{16}$$

Forrestal et al. (1994, 1996), Frew et al. (1998) (see also Li and Chen, 2003) studied the validity of this model and the range of velocities when it can be applied for the concrete shields. The conclusion is that "predictions... are in good agreement with (experimental) data until nose erosion becomes excessive" (Forrestal et al., 1996). Experiments confirmed good performance of the model up to the impact velocities of 800 m/s, and feasibility to apply it (although with care) at higher velocities up to 1200 m/s. For the limestone shields the model is quite accurate in the whole studied range of the impact velocities, up to 1650 m/s (Frew et al., 2000; Forrestal and Hanchak, 2002).

We consider the problem of maximizing DOP H for the semi-infinite target with known parameters determining its mechanical properties, namely, γ and f_c' (for a concrete target). The mass of the impactor m, the length L and shank radius R of the nose of the projectile are assumed to be given. The problem is to determine a maximum of the functional H in Eq. (15) taking into account the following condition:

$$\Phi(L)=R. \tag{17}$$

3. Optimum nose geometry

3.1. A property of the criterion functional

Eq. (15) and associated with this criterion functional H, Eqs. (5), (6), (8) and (16), do not contain the unknown parameter r explicitly and the shape of the impactor, for a given L and R, is described only by integral J. Using the expression for H in Eq. (15) and Eqs. (6) and (16) allows us to determine the derivative

$$\frac{\mathrm{d}H}{\mathrm{d}J}=\frac{\mathrm{d}H}{\mathrm{d}b}\cdot\frac{\mathrm{d}b}{\mathrm{d}J}=-2\pi b_0\frac{\mathrm{d}H}{\mathrm{d}b}=-\pi b_0 m\left[-\int_0^{\hat{w}}\frac{w\,\mathrm{d}w}{(a+bw)^2}-\frac{1}{a+b\hat{w}}\cdot\frac{4R(mv_0^2-4aR)}{(m+4bR)^2}\right]>0. \tag{18}$$

Here we used formula from Korn and Korn (1968) to calculate a derivative of an integral over a parameter when a function and the upper limit in the integral depend upon this parameter. Thus H is an increasing function of J and the problem is reduced to the problem of maximization of functional J.

Using dimensionless variables

$$\bar{x}=\frac{x}{L},\quad \overline{\Phi}=\frac{\Phi}{L},\quad \dot{\overline{\Phi}}=\frac{\mathrm{d}\overline{\Phi}}{\mathrm{d}\bar{x}},\quad \tau=\frac{R}{L}, \tag{19}$$

$$\overline{H}=\frac{H}{2R},\quad k_1=\frac{mv_0^2}{4\pi a_0R^3}-1,\quad k_2=\frac{m}{4\pi b_0RL^2}, \tag{20}$$

Eq. (15) can be rewritten as follows:

$$\overline{H} = \Psi(k_1, k_2\overline{M}) = 2 + k_2\overline{M}\mathrm{Ln}\left(1 + \frac{k_1}{k_2\overline{M} + 1}\right), \tag{21}$$

where

$$\overline{M} = \frac{1}{\tau^2 - 2\overline{J}}, \tag{22}$$

$$\overline{J} = \int_0^1 \frac{\overline{\Phi}\dot{\overline{\Phi}}}{\dot{\overline{\Phi}}^2 + 1}\mathrm{d}\bar{x}. \tag{23}$$

In dimensionless variables, the problem is to minimize the functional $\overline{J}$ with the condition:

$$\overline{\Phi}(1) = \tau. \tag{24}$$

3.2. "Absolute optimum" nose geometry

Since the problem of maximization of the functional $\overline{J}$ is equivalent to the problem of minimization of the functional $\overline{I} = \tau^2 - 2\overline{J}$, we can use the results of Eggers and Resnikoff (1957) (see also Miele, 1965) where the latter variational problem was solved, and to write the solution of our problem as follows:

$$\bar{x}(t) = \bar{r}_{\mathrm{opt}}A(t), \quad \overline{\Phi}(t) = \bar{r}_{\mathrm{opt}}B(t), \quad \bar{r}_{\mathrm{opt}} = \frac{r_{\mathrm{opt}}}{L} = \frac{1}{A(t_0)}, \quad t_0 \leqslant t \leqslant 1, \tag{25}$$

where r_{opt} is the radius of the flat bluntness of the optimal impactor,

$$A(t) = \frac{1}{4}\left(\frac{1}{t^2} + \frac{3}{4t^4} + \ln t - \frac{7}{4}\right), \qquad B(t) = \frac{(t^2+1)^2}{4t^3}, \tag{26}$$

the parameter t_0 satisfies the equation

$$B(t_0) - \tau A(t_0) = 0, \tag{27}$$

whose solution is showed in Fig. 2. The shape of the generator of the optimal impactor is shown in Fig. 3 for different τ. The optimum impactor has a flat bluntness with a shank radius ratio r_{opt}/R that increases when τ is increased.

The maximum value of the functional $\overline{J}$ is

$$\overline{J}_{\mathrm{opt}} = \frac{\tau^2 C(t_0)}{8B^2(t_0)}, \qquad C(t) = \frac{1}{2t^2} + \frac{5}{4t^4} + \frac{1}{2t^6} + \ln t - \frac{9}{4}. \tag{28}$$

The dependence of the maximum value of $\overline{J}$ as a function of τ is shown in Fig. 11.

Let us determine the optimal geometry of impactors for some simple classes of shapes and analyze their efficiency as compared to the absolute optimum impactor.

3.3. Optimum truncated-conic nose

The equation of the generator of truncated-conic impactor's nose reads:

$$\overline{\Phi}(\bar{x}) = \bar{r} + \tan\alpha\bar{x}, \quad \bar{r} = \tau - \tan\alpha, \quad \bar{r} = r/L, \tag{29}$$

where α is an angle between the generator and $\bar{x}$-axis. Substituting the latter equations into Eq. (23) we find that

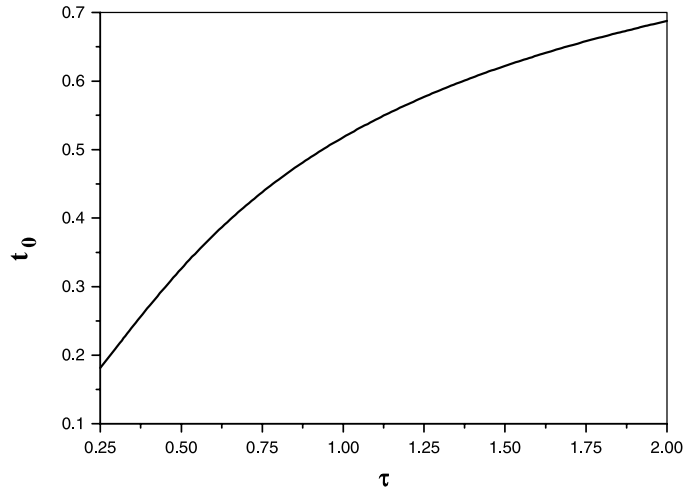

Fig. 2. Solution of Eq. (27) in graphical form.

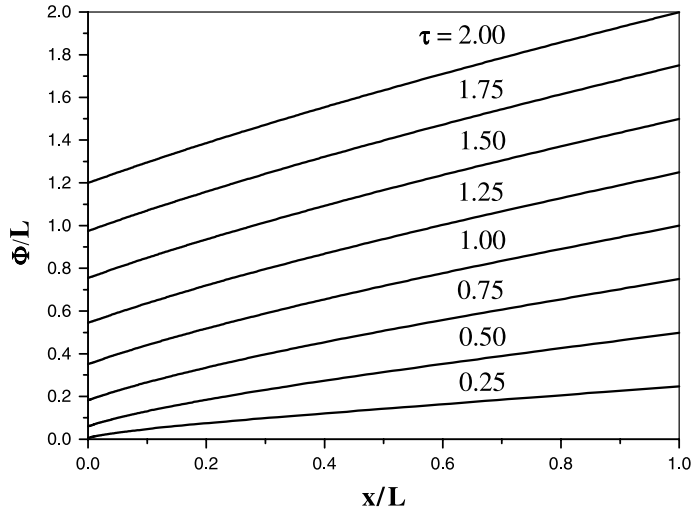

Fig. 3. Shape of the generator of the optimal impactor.

$$\overline{J} = \sin\alpha(\tau\cos\alpha - 0.5\sin\alpha), \quad 0 \leqslant \tan\alpha \leqslant \tau. \tag{30}$$

The minimum of the function $\overline{J} = \overline{J}(\alpha)$ is attained when (Ben-Dor et al., 2001)

$$\alpha = \alpha_* = \frac{1}{2}\tan^{-1}(2\tau) \tag{31}$$

and the optimal radius of the bluntness $r_{\text{opt cone}}$ and the optimal value of the functional $\overline{J}$, $\overline{J}_{\text{opt cone}}$ read:

$$\frac{r_{\text{opt cone}}}{R} = 1 - \frac{2}{\sqrt{4\tau^2+1}+1}, \qquad \overline{J}_{\text{opt cone}} = \frac{1}{4}\left(\sqrt{4\tau^2+1}-1\right). \tag{32}$$

For a sharp cone $\tan\alpha = \tau$ and Eq. (30) yields the following formula for the value of the functional $\overline{J}$:

$$\overline{J} = \overline{J}_{\text{sh cone}} = \frac{\tau^2}{2(\tau^2+1)}. \tag{33}$$

The plots of $\overline{J}$ versus $\tilde{r} = r/R$ for different τ are shown in Fig. 4. The variation of the function is quite small in the neighborhood of the maximum, most notably for relatively small τ. This means that the radius of the flat bluntness can be changed in the vicinity of the optimal value (see Fig. 5) without considerable loss in value of the integral $\overline{J}$. The plots of $\overline{J}$ versus τ for optimal truncated cone and sharp cone are shown in Fig. 11.

3.4. Optimum truncated-ogive nose

The equation of the generator of truncated-ogive impactor's nose read:

$$\overline{\Phi}(\bar{x}) = \tau - \bar{\rho}_* + \sqrt{\bar{\rho}_*^2 - (\bar{x}-1)^2}, \quad \bar{\rho}_* = \rho_*/L, \quad 0 \leqslant \bar{x} \leqslant 1, \tag{34}$$

where ρ_* is the ogive radius,

$$\bar{\rho}_* = \frac{(\tau-\bar{r})^2+1}{2(\tau-\bar{r})} \tag{35}$$

and the conditions that follows from geometrical considerations must be satisfied:

$$\tau^2 - 1 \leqslant \bar{r}^2 \leqslant \tau^2, \quad \text{or } 1-\tau^{-2} \leqslant \tilde{r}^2 \leqslant 1, \quad \tilde{r} = r/R. \tag{36}$$

Substituting Eq. (34) into Eq. (23) we find that

$$\overline{J} = \frac{1}{2} + \frac{\tau-\bar{\rho}_*}{3\bar{\rho}_*^2}[\bar{\rho}_*^3 - (\bar{\rho}_*^2-1)^{3/2}] - \frac{1}{4\bar{\rho}_*^2}. \tag{37}$$

In the case of the ogive-nose impactor without flat bluntness, $r = 0$ and Eqs. (35) and (37) can be rewritten as

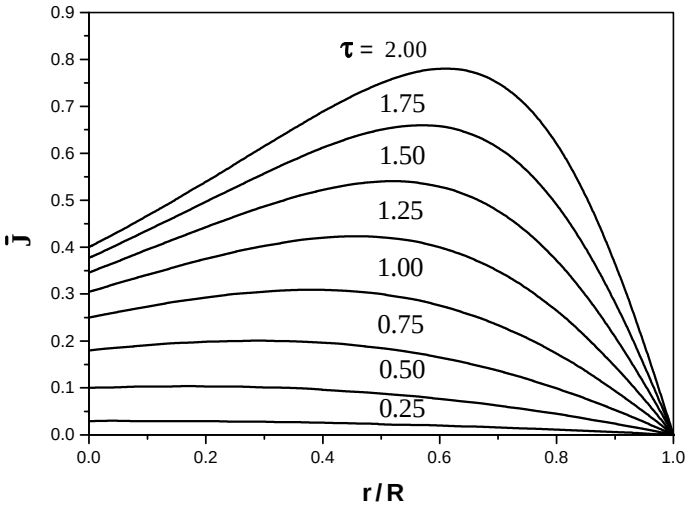

Fig. 4. Functional $\overline{J}$ versus relative radius of the bluntness of truncated-conic impactor.

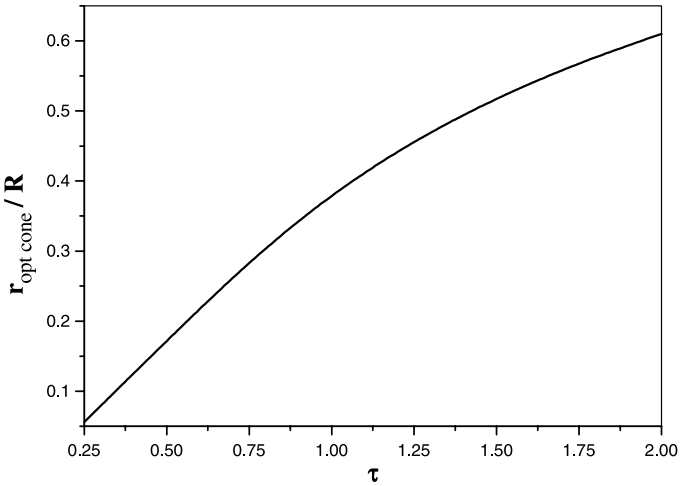

Fig. 5. Relative radius of the bluntness of the optimum truncated-conic impactor versus given relative thickness.

$$\bar{\rho}_* = \frac{\tau^2+1}{2\tau}, \quad \overline{J} = \frac{\tau^2(\tau^4+2\tau^2+3)}{6(\tau^2+1)^2}, \quad \tau \leqslant 1. \tag{38}$$

Using the caliber-radius-head parameter

$$\psi = \frac{\rho_*}{2R} = \frac{\bar{\rho}_*}{2\tau} = \frac{\tau^2+1}{4\tau^2}, \tag{39}$$

the second in Eq. (38) can be rewritten as

$$\overline{J} = \frac{24\psi^2 - 8\psi + 1}{48\psi^2(4\psi-1)}, \qquad \psi \geqslant \frac{1}{2}. \tag{40}$$

The plots of $\overline{J}$ versus $\tilde{r}$ for different τ are shown in Fig. 6. If $\tau \leqslant 1$ then $\tilde{r}$ changes from 0 to 1; there is a maximum $\overline{J}(\tilde{r})$ but the values of the function are very close to this maximum value when $\tilde{r}$ changes in the range from 0 to 0.5. If $\tau > 1$ then $\tilde{r}$ changes from $\tilde{r}_0 = \sqrt{1-\tau^{-2}}$ to 1. If $1 < \tau <\approx 1.15$ then the maximum $\overline{J}(\tilde{r})$ is attained for $\tilde{r} > \tilde{r}_0$, if $\tau >\approx 1.15$ then $\tilde{r} = \tilde{r}_0$ is the point of the maximum $\overline{J}(\tilde{r})$. The plots of $\overline{J}$ versus $\tilde{r}$ becomes progressively less flattened curves with increasing τ. The plots of the optimal $\tilde{r}$ and the maximum $\overline{J}$ versus τ are shown in Figs. 7 and 11, respectively.

3.5. Optimum spherical-conic nose

The equation of the generator of spherical-conic impactor's nose (see Fig. 8) reads:

$$\overline{\Phi}(\bar{x}) = \begin{cases} \sqrt{(2\bar{\rho}-\bar{x})\bar{x}} & \text{if } 0 \leqslant \bar{x} \leqslant \bar{x}_0, \\ \rho\cos\alpha + tg\alpha(\bar{x}-\bar{x}_0) & \text{if } \bar{x}_0 \leqslant \bar{x} \leqslant 1, \end{cases} \tag{41}$$

where ρ is the radius of spherical bluntness, α is the angle between the generator of the cone and $\bar{x}$-axis,

$$\bar{x}_0 = \frac{x_0}{L} = \tau\cos\alpha - \sin\alpha, \qquad \bar{\rho} = \frac{\rho}{L} = \frac{\bar{x}_0}{1-\sin\alpha} \tag{42}$$

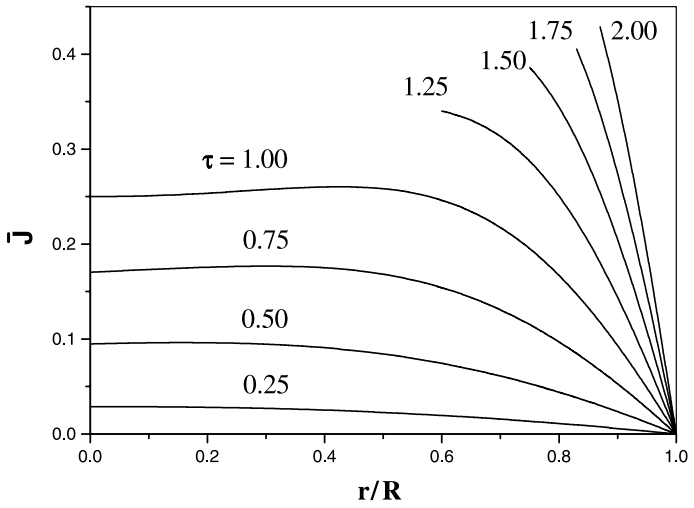

Fig. 6. Functional $\bar{J}$ versus relative radius of the bluntness of truncated-ogive impactor.

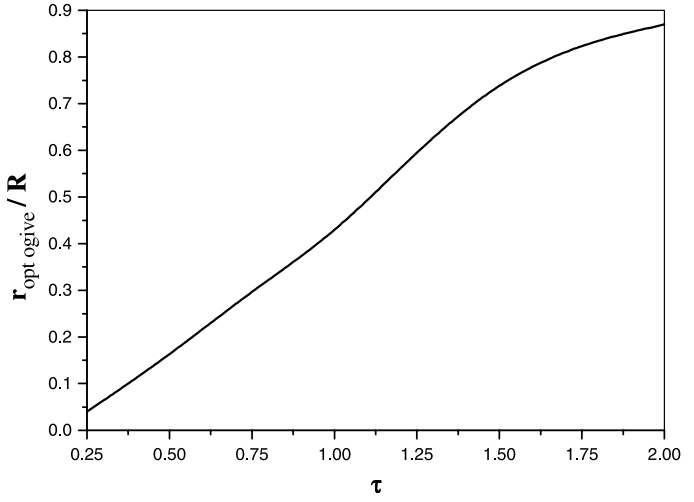

Fig. 7. Relative radius of the bluntness of the optimum truncated-ogive impactor versus given relative thickness.

and the following conditions that follow from geometrical considerations must be satisfied:

$$0 \leqslant \bar{\rho} \leqslant \min(1, \tau), \quad \text{or } 0 \leqslant \tilde{\rho} \leqslant \min(\tau^{-1}, 1) \quad \tilde{\rho} = \rho/R. \tag{43}$$

Substituting Eq. (41) into Eq. (23) we find that

$$\overline{J} = 0.25\bar{\rho}^2 \cos^4 \alpha + 0.5 \sin \alpha (1 - \bar{x}_0)[2\bar{\rho} \cos^2 \alpha + (1 - \bar{x}_0) \sin \alpha]. \tag{44}$$

The plots of $\overline{J}$ versus $\tilde{\rho}$ for different τ are shown in Fig. 9. If $\tau \leqslant 1$ then $\tilde{\rho}$ changes from 0 to 1; there is a maximum $\overline{J}(\tilde{\rho})$ but variation of the function is quite small in the neighborhood of the maximum. If $\tau > 1$ then $\tilde{\rho}$ varies from 0 to $\tilde{\rho}_0 = \tau^{-1}$. If $1 < \tau <\approx 1.2$ then the maximum $\overline{J}(\tilde{\rho})$ is attained for $\tilde{\rho} < \tilde{\rho}_0$, if $\tau >\approx 1.2$

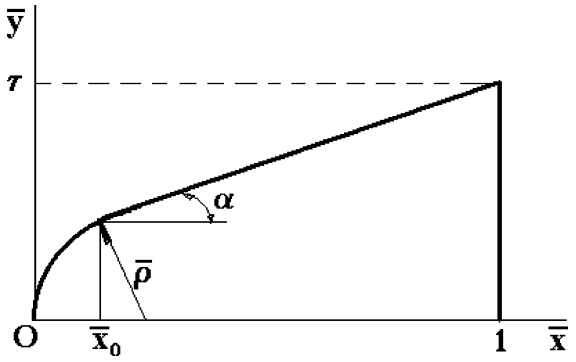

Fig. 8. The shape of spherical-conic impactor.

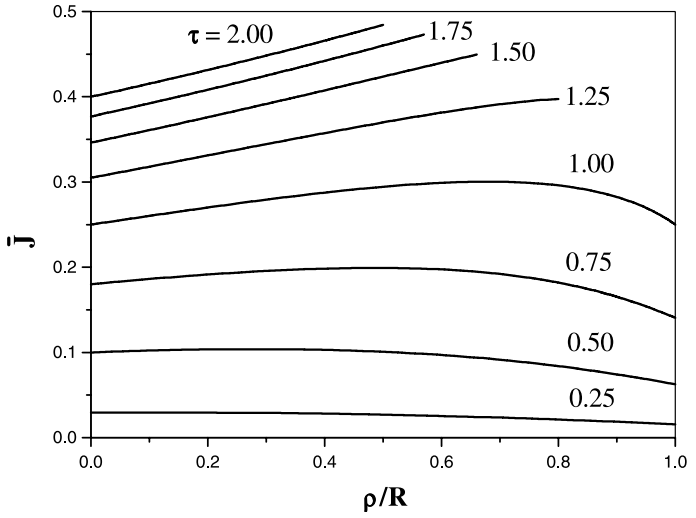

Fig. 9. Functional $\overline{J}$ versus relative radius of the spherical bluntness of spherical-conic impactor.

then $\tilde{\rho} = \tilde{\rho}_0$ is the point of the maximum $\overline{J}(\tilde{\rho})$. The plots of the optimal $\tilde{\rho}$ and maximum $\overline{J}$ versus τ are shown in Figs. 10 and 11, respectively.

3.6. Comparison of different nose shapes

The plots of the maximum $\overline{J}$ versus τ are shown in Fig. 11 for the absolute optimal nose and the optimal noses among the considered nose shapes. It is seen from Eq. (23) that minimum $\overline{J}$ is 0, and this value is attained for the cylinder, $\overline{\Phi}(\bar{x}) = \tau$.

First and foremost, it is shown in Fig. 11 that the functional $\overline{J}$ for optimal truncated-conic nose assumes the values that are very close to the optimum for all τ. For $0 < \tau <\approx 0.5$, the difference in the values $\overline{J}$ for all shapes is very small. For $\approx 0.5 < \tau <\approx 1.0$, value of $\overline{J}$ for the optimum spherical-conic nose is close to the optimum. For relatively large τ, the advantage of the absolute optimal nose and the optimal truncated-conic nose over other shapes becomes quite essential.

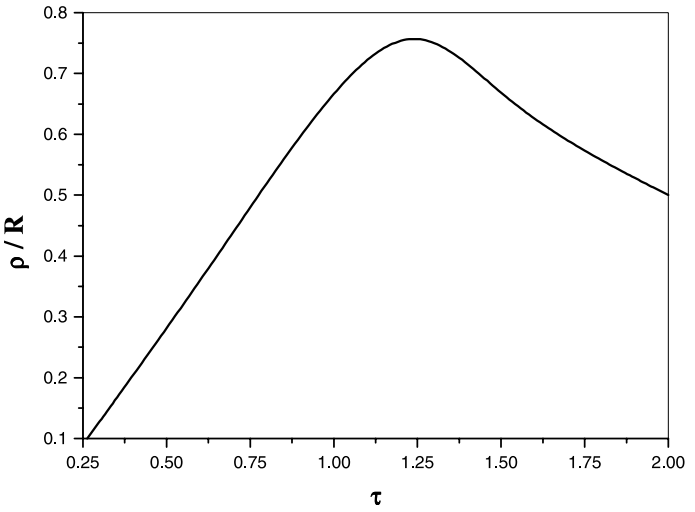

Fig. 10. Relative radius of the bluntness of the optimum spherical-conic impactor versus given relative thickness.

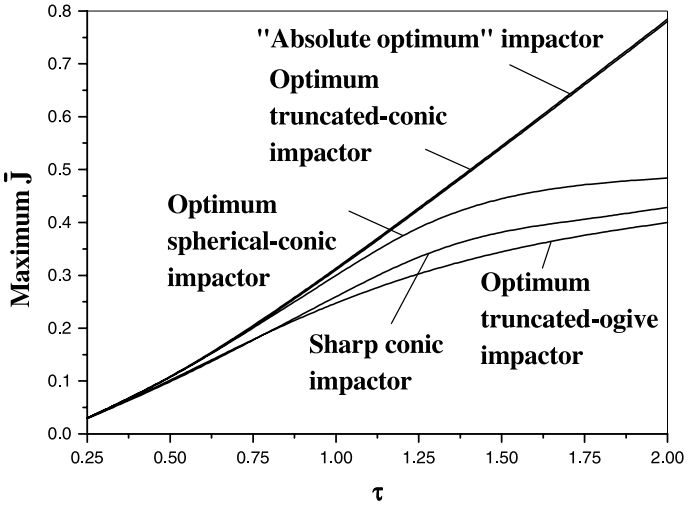

Fig. 11. Comparison of performance of impactors with different shapes of the nose.

Generally, the difference in the magnitude of the functional $\overline{J}$ cannot be considered as a measure of the difference in the criterion of optimization. In order to compare the efficiencies of the 'absolute optimal' impactor and the optimal truncated-conic impactor the following index

$$\varepsilon_0 = \frac{H_{\text{opt}} - H_{\text{opt cone}}}{H_{\text{opt}}} \times 100\%, \tag{45}$$

is used, where H_{opt} and $H_{\text{opt cone}}$ are DOP of the 'absolute optimum' impactor and optimum truncated-conic impactor, respectively. Figs. 12a–d show that these impactors are practically equivalent. This property allows us to propose the approximate analytical formula for the ''absolute maximum'' DOP, namely,

$$\overline{H}_{\max} = \Psi(k_1, k_2\overline{M}_*), \tag{46}$$

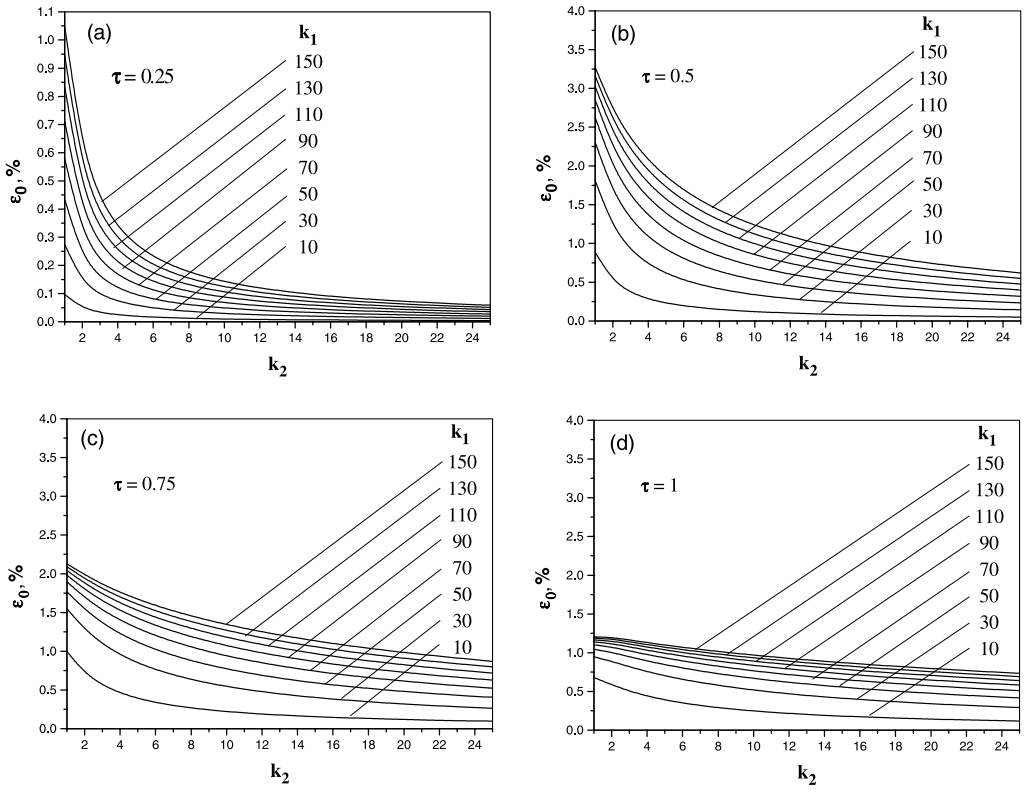

Fig. 12. (a–d) Comparison of performance of the optimum truncated-conic impactor and the "absolute optimum" impactor.

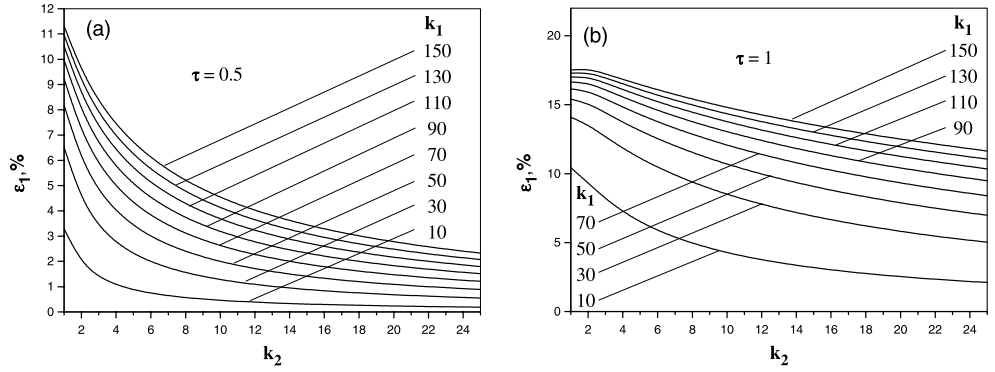

Fig. 13. (a, b) Comparison of performance of the sharp conic impactor and the "absolute optimum" impactor.

where Ψ is determined by Eq. (21) and $\overline{M}$ is calculated using the second in Eqs. (32) for the optimum truncated-conic impactor:

$$\overline{M}_* = \frac{1}{\tau^2 - 2\overline{J}_{\text{opt cone}}} = \frac{2\tau^2 + 1 + \sqrt{4\tau^2 + 1}}{2\tau^4}. \tag{47}$$

The "absolute optimum" impactor and the sharp conic impactor are compared in Fig. 13a and b using the index:

$$\varepsilon_1 = \frac{H_{\text{opt}} - H_{\text{sh cone}}}{H_{\text{opt}}} \times 100\%. \tag{48}$$

The pronounced advantage of the optimal shape over the sharp cone is clearly demonstrated in these figures.

4. Concluding remarks

We determined the shape of the normally striking impactor penetrating to the maximum depth into a concrete or a limestone semi-infinite target. The optimal shape is independent on the properties of the material of the target in the framework of the employed model of penetration. The optimum impactor has a flat bluntness, its shape and DOP are very close to the shape and DOP of the optimal truncated-conic impactor. The typical shapes of the impactors in order of decreasing DOP, are optimal truncated-conic impactor, optimal spherical-conic impactor, sharp-conic impactor, and optimal truncated-ogive impactor. The difference in efficiency between the optimal impactor or the optimal truncated-conic impactor and each of the remaining impactors in the list increases with increase of the thickness of the impactor.

Although in this study we employed a penetration model that was validated experimentally further experimental studies should be performed with the end to analyze theoretical predictions. In these experiments parameters k_1, k_2, τ must be kept constant when changing the shape of the impactor since they were assumed constant in the theoretical study of the optimization problem. We consider the results of our theoretical analysis as a basis and a stimulus for further experimental investigations.

References

Ben-Dor, G., Dubinsky, A., Elperin, T., 1997. Optimal 3D impactors penetrating into layered target. Theoretical and Applied Fracture Mechanics 27, 161–166.

Ben-Dor, G., Dubinsky, A., Elperin, T., 1999. Some ballistic properties of non-homogeneous shields. Composites A 30, 733–736.

Ben-Dor, G., Dubinsky, A., Elperin, T., 2000. Optimization of the shape of a penetrator taking into account plug formation. International Journal of Fracture 106, L29–L34.

Ben-Dor, G., Dubinsky, A., Elperin, T., 2001. Shape optimization of penetrator nose. Theoretical and Applied Fracture Mechanics 35, 261–270.

Ben-Dor, G., Dubinsky, A., Elperin, T., 2002a. Optimal nose geometry of the impactor against FRP laminates. Composite Structures 55, 73–80.

Ben-Dor, G., Dubinsky, A., Elperin, T., 2002b. Optimization of the nose shape of an impactor against a semi-infinite FRP laminate. Composite Science and Technology 62, 663–667.

Ben-Dor, G., Dubinsky, A., Elperin, T., 2003. Numerical solution for shape optimization of an impactor penetrating into a semi-infinite target. Computers and Structures 81 (1), 9–14.

Bunimovich, A.I., Dubinsky, A., 1995. Mathematical Models and Methods of Localized Interaction Theory. World Scientific Publishing Company, Singapore.

Bunimovich, A.I., Yakunina, G.E., 1987a. The shapes of three-dimensional minimum-resistance bodies moving in compressible plastic and elastic media. Moscow University Mechanics Bulletin 42, 59–62.

Bunimovich, A.I., Yakunina, G.E., 1987b. On the shape of minimum-resistance solids of revolution moving in plastically compressible and elastic-plastic media. Journal of Applied Mathematics and Mechanics 51, 386–392.

Bunimovich, A.I., Yakunina, G.E., 1989. On the shape of a minimum resistance solid of rotation penetrating into plastically compressible media without detachment. Journal of Applied Mathematics and Mechanics 53, 380–683.

Chen, X.W., Li, Q.M., 2001. Deep penetration of truncated-ogive-nose projectile into concrete targets. In: Proceeding of the 4th International Symposium on Impact Engineering, Kumamoto, Japan.

Chen, X.W., Li, Q.M., 2002. Deep penetration of a non-deformable projectile with different geometrical characteristics. International Journal of Impact Engineering 27, 619–637.

Eggers Jr., A.J., Resnikoff, M.M., Dennis, D.H., 1957. Bodies of revolutions having minimum-drag at high supersonic airspeeds. NACA, Rep. 1306.

Forrestal, M.J., Luk, V.K., 1992. Penetration into soil targets. International Journal of Impact Engineering 12 (3), 427–444.
Forrestal, M.J., Hanchak, S.J., 2002. Penetration limit velocity for ogive-nose projectiles and limestone targets. Transactions of ASME, Journal of Applied Mechanics 69, 853–854.
Forrestal, M.J., Altman, D.S., Cargile, J.D., Hanchak, S.J., 1994. An empirical equation for penetration depth of ogive-nose projectiles into concrete targets. International Journal of Impact Engineering 15 (4), 395–405.
Forrestal, M.J., Frew, D.J., Hanchak, S.J., Brar, N.S., 1996. Penetration of grout and concrete targets with ogive-nose steel projectiles. International Journal of Impact Engineering 18 (5), 465–476.
Frew, D.J., Hanchak, S.J., Green, M.L., Forrestal, M.J., 1998. Penetration of concrete targets with ogive-nose steel rods. International Journal of Impact Engineering 21 (6), 489–497.
Frew, D.J., Forrestal, M.J., Hanchak, S.J., 2000. Penetration experiments with limestone targets and ogive-nose steel projectiles. Transactions of ASME 67, 841–845.
Jones, S.J., Rule, W.K., 2000. On the optimal nose geometry for a rigid penetrator, including the effects of pressure-dependent friction. International Journal of Impact Engineering 24, 403–415.
Jones, S.J., Rule, W.K., Jerome, D.M., Klug, R.T., 1998. On the optimal nose geometry for a rigid penetrator. Computational Mechanics 22, 413–417.
Korn, G.A., Korn, T.M., 1968. Mathematical Handbook for Scientists and Engineers. McGraw-Hill Book Company, New York.
Kusher, V., 1967. Penetration with optimal work. Ballistic Research Laboratory, Aberdeen Proving Ground, Maryland, USA, BRL-R-1384 (AD 664138).
Li, Q.M., Chen, X.W., 2003. Dimensionless formulae for penetration depth of concrete target impacted by a non-deformable projectile. International Journal of Impact Engineering 28, 93–116.
Miele, A. (Ed.), 1965. Theory of Optimum Aerodynamic Shapes. Academic Press, New York.
Nixdorff, K., 1987. On the efficiency of different head shapes to perforate thin targets. Transactions of CSME 11, 109–112.
Ostapenko, N.A., Yakunina, G.E., 1992. Least-drag bodies moving in media subject to locality hypothesis. Fluid Dynamics 27, 71–80.
Ostapenko, N.A., Yakunina, G.E., 1999. The shape of slender three-dimensional bodies with maximum depth of penetration into dense media. Journal of Applied Mathematics and Mechanics 63, 953–967.
Ostapenko, N.A., Romanchenko, V.L., Yakunina, G.E., 1994. Optimum forms of three-dimensional bodies for penetration of dense media. Journal of Applied Mechanics and Technical Physics 4, 515–521.
Qian, L., Yang, Y., Liu, T., 2000. A semi-analytical model for tuncated-ogive-nose projectiles penetration into semi-infinite concrete targets. International Journal of Impact Engineering 24, 947–955.
Vedernikov, Y.A., Shchepanovsly, V.A., 1995. Optimization of Reagasdynamic Systems. Nauka, Novosibirsk.
Yakunina, G.E., 2000. The construction of three-dimensional shapes within the framework of a model of lical interaction. Journal of Applied Mathematics and Mechanics 64, 289–298.
Yakunina, G.E., 2001. On body shapes providing maximum penetration depth in dense media. Doklady Physics 46, 140–143.
Yankilevsky, D.Z., 1983. The optimal shape of an earth penetrating projectile. International Journal of Solids and Structures 19, 25–31.